



OPEN

## Synergetic effect of essential oils and calcium phosphate nanoparticles for enhancement the corrosion resistance of titanium dental implant

Heba Tarek Zaher<sup>2</sup>, Mahmoud A. Hefnawy<sup>1</sup>, Shymaa S. Medany<sup>1</sup>, S. M. Kamel<sup>3</sup> & Sahar A. Fadlallah<sup>1,2</sup>✉

Calcium phosphate ( $\text{CaPO}_4$ ) coating is one of various methods that is used to modify the topography and the chemistry of Ti dental implant surface to solve sever oral problems that result from diseases, accidents, or even caries due to its biocompatibility. In this work, anodized (Ti-bare) was coated by  $\text{CaPO}_4$  prepared from amorphous calcium phosphate nanoparticles (ACP-NPs) and confirmed the structure by X-ray diffraction (XRD) and Fourier-transform infrared spectroscopy (FT-IR) techniques. Ti-bare was coated by prepared  $\text{CaPO}_4$  through the casting process, and the morphology of Ti/ $\text{CaPO}_4$  was characterized by scanning electron microscope (SEM) where the nano-flakes shape of  $\text{CaPO}_4$  and measured to be 60–80 nm was confirmed. The stability of Ti-bare and coated Ti/ $\text{CaPO}_4$  was studied in a simulated saliva solution using electrochemical impedance spectroscopy (EIS) and linear polarization techniques to deduce their corrosion resistance. Furthermore, three essential oils (EO), Cumin, Thyme, and Coriander, were used to stimulate their synergistic effect with the  $\text{CaPO}_4$  coat to enhance the corrosion resistance of Ti implant in an oral environment. The fitting EIS parameters based on  $R_s [R_{ct}C] W$  circuit proved that the charge transfer resistance ( $R_{ct}$ ) of Ti/ $\text{CaPO}_4$  increased by 264.4, 88.2, and 437.5% for Cumin, Thyme, and Coriander, respectively, at 2% concentration.

Millions of people worldwide are affected by dental caries, a chronic disease with high prevalence. The first stage of dental caries appears as white spots that form non-cavitated lesions, and the second stage is carious cavities. Once dental caries occurs, it will be hard to reverse or stop it from progressing. The ultimate objective is to stop the caries process using non-invasive methods at that white spot lesion stage. There are different conventional techniques for caries removal, but the most famous one is Chemo-mechanical caries removal. After the caries get removed, composite material to fill the teeth is necessary. A composite that can strongly bond with the teeth to form the best adherence ability is considered one of the important abilities needed for a successful restoration process<sup>1–4</sup>. Caries may appear during orthodontic treatments, from the enamel to leak—cavitation that leads to loss of minerals, primarily calcium and phosphorus loss. Therefore, special composite can be used on the labial surfaces or banded teeth through enamel decalcification and remineralization<sup>5</sup>. Amorphous Calcium phosphate (ACP) is a promising compound that can release calcium and phosphate for the prevention and treatment of decalcification. At the same time, ACP nanoparticle (ACP-NPs) have recently attracted much attention because of their outstanding performance and unique area that enhances the stability of implant metal in the oral environment<sup>6</sup>.

Titanium and its alloys are used as dental implants to solve the severe oral problems that result from diseases, accidents, or even caries due to their fascinating properties like excellent biocompatibility, high corrosion resistance, acceptable strength-to-weight ratio, low elastic modulus, and low density<sup>7–11</sup>. Based on the chemistry of the titanium surface, which is naturally oxidized and covered with a thin layer from titania ( $\text{TiO}_2$ ), through the anodization process, the thin  $\text{TiO}_2$  layer is enlarged in its thickness to enhance the biocompatibility of Ti implant in physiological solution<sup>12</sup>.  $\text{TiO}_2$  layer is easily hydrated when exposed to an aqueous medium, and the

<sup>1</sup>Chemistry Department, Faculty of Science, Cairo University, Giza 12613, Egypt. <sup>2</sup>Biotechnology Department, Faculty of Science, Cairo University, Giza 12613, Egypt. <sup>3</sup>Oral Biology, October University for Modern Sciences and Art, MSA University, Giza, Egypt. ✉email: sahar.fadlallah@yahoo.com; sahmed@sci.cu.edu.eg

developing hydroxyl functional group will improve the chemical activity toward other ions such as phosphate and calcium<sup>13</sup>. Furthermore, calcium phosphate was reported as an effective coat for anodized Ti metal and its alloys<sup>16–18</sup> and other biomaterial metals such as Mg, Zn, Sr, Ca, Ag, and Zr<sup>14–17</sup>, due to the obtaining of morphology and chemical structure similar to natural bone.

Plants contain compounds like carotenoids, phenols, vitamins, and flavonoids that reduce agents<sup>18–20</sup>. Plant extract products, such as essential oils, are used in tiny concentrations to protect the surface of metals from corrosive environments. The plant extracts can also be considered site blockers or adsorption site blockers because of their ability to absorb on the metal surface. Herbal extracts can be used as an early intervention strategy to manage caries, using as grape seeds, cinnamon oil, tea tree oil, and garlic extract are receiving more attention for their use as phytotherapy is preferred due to their biocompatibility and effectiveness. These extracts have been found to have strong antimicrobial and preventive effects on synthetic antibiotics<sup>21</sup>. In another perspective, several natural products were reported in the literature as effective green protective solutions, such as *Delonix regia*; rosemary leaves extracts that inhibited the corrosion of aluminum, natural honey for inhibition of copper corrosion, and African bush pepper; neem leaves; *Carica papaya* leaves extract for inhibition of mild steel corrosion<sup>22–27</sup>. However, the organic compounds' effectiveness regards the molecular chemical formula and its related physicochemical properties of the compound, like the presence of donor/ acceptor atoms and the extended functional groups<sup>28,29</sup>. Additionally, these natural compounds support the stability of the metal by adsorption or forming protective barrier films on the metal surface<sup>22</sup>.

Cumin (*Cuminum cyminum* L.) is a member of the Apiaceae family that spread through Mediterranean region, Middle East, and India. It considered as traditional medicine due to various active ingredients like terpenes, phenols, and flavonoids<sup>30–32</sup>. Thus, the presence of phenolic compound in Cumin leads to enhance the anti-corrosion ability as reported for different metals and alloys like aluminum, copper, and steel<sup>33–35</sup>.

Thyme (*Thymus vulgaris* L.) is considered as a member of the Lamiaceae family, Whereas the Thyme is widely spread economically in North America, Europe, and North Africa<sup>36</sup>. Due to the presence of aromatic compound, the Thyme plant extract was observed to have high effectiveness toward corrosion of different Alloys like mild steel, and 304 steel<sup>37–39</sup>.

Coriander (*Coriandrum sativum* L.) contains essential oils in its leaves, flowers and seeds. Thus the coriander is considered as member of the Apiaceae family, is among most widely used medicinal plant, possessing nutritional as well as medicinal properties. The *Coriandrum* is widely reported in literature as green corrosion inhibitor for several metals and alloys like aluminum, mild steel, 6063 aluminum alloy, and carbon steel<sup>40–43</sup>.

Electrochemical impedance spectroscopy (EIS) is one of the most powerful techniques widely used to estimate the electrochemical behavior of the metals in the electrolytic solutions to characterize various electrochemical systems<sup>44–50</sup>. Thus, it shows and deduces the contribution between the metal surface and the electrolytic solution under electrochemical conditions. Furthermore, it can be used for simulating the dynamics of active mobile charge in the interface regions by fitting the out-put EIS data into different impedance parameters<sup>51–58</sup>.

In the present work, a new comparative study was performed on Ti- bare and coated Ti/CaPO<sub>4</sub> samples to deduce the positive impact of CaPO<sub>4</sub> under the synergistic effect of essential oils, where they act together for enhancement of the corrosion resistance of Ti dental implant in simulated oral solution. Ti/CaPO<sub>4</sub> sample was soaked in the saliva solution for different intervals periods of up to 14 days to determine the change in charge transfer resistance, corresponding to the corrosion resistance, with time. Furthermore, Cumin, Thyme, and Coriander oils were added to the artificial physiological solution to deduce the synergistic relation of each with the CaPO<sub>4</sub> coat and its positive impact on the implant surface. Also, the linear polarization technique was employed to measure the impact of oil on the corrosion process, and the corrosion rates of Ti-bare and coated Ti/CaPO<sub>4</sub> were studied. Otherwise, the comparison between different oils.

## Experimental work

### Anodization

Through the anodization process, the layer of TiO<sub>2</sub> was formed as follows: the Ti-foil with an area of 1 cm × 1 cm and thickness of 1mm (99.99% metal basis, Sigma Aldrich) was used as the starting material. First, the Ti degreasing was performed by sonication in a mixture of acetone, isopropanol, and methanol. Then, the foil was washed with deionized water and dried in nitrogen steam. The Ti sample was connected at the positive pole of the power supply and immersed in a solution of 1.0 M H<sub>3</sub>PO<sub>4</sub> + 0.8 wt.% NaF doing as oxidants in the electrochemical cell at a constant potential of 20 V for 30 min. Finally, the sample after anodization was cleaned by immersion several times in deionized water and dried overnight in an oven under a nitrogen atmosphere, and then the Ti-bare sample was ready. The main goals for surface treatment through anodization are enhancement of bioactivity, biocompatibility, and corrosion resistance for dental applications.

### Preparation of ACP-NPs

Potassium hydrogen phosphate was dissolved in deionized water at room temperature, along with the addition of calcium nitrate to form a P-precursor Ca-precursor solution with concentrations 0.040 M and 0.036 M, respectively. The pH value of the solution was fixed and adjusted at 8.0 by appending ammonium hydroxide solution (0.1 M) while continuously stirring at room temperature (25 °C) until a white slurry formation was achieved. The solution was centrifuged at 7000 rpm for 10 min and washed with distilled water three times. The prepared calcium phosphate precipitate was washed with acetone three times and dried at room temperature for 24 h; they were later stored under a vacuum for chemical structure characterization by XRD & FT-IR and further electrochemical studies.

## Electrochemical measurements of prepared Ti/CaPO<sub>4</sub>

To produce a new modified Ti implant surface by ACP-NPs and subsequently evaluate its electrochemical behavior, a working electrode was utilized in the experiment. It consisted of an anodized sample Ti-bare with a surface area of 0.0625 cm<sup>2</sup> and a thickness of 1 mm. Initially, the surface underwent a polishing process utilizing a gentle emery paper, followed by a thorough rinse with double distilled water and ethanol.

The ACP-NPs were prepared from 50 mg calcium triphosphate and suspended in 1 mL of ethanol. The 100 μL of suspension was cast on the anodized Ti-bare surface. Finally, the surface was dried overnight. The samples were nominated by Ti/CaPO<sub>4</sub> when not exposed to the essential oils, but when exposed to EO named based on the type of the oil used as Ti/CaPO<sub>4</sub>-L1, Ti/CaPO<sub>4</sub>-L2, and Ti/CaPO<sub>4</sub>-L3 for Cumin, Thyme, and Coriander oils, respectively. The essential oils were supplied by local brand “Harraz” the concentration of pure essential oil is ~ 100%.

EIS and polarization results were achieved using Autolab PGSTAT128N. The electrochemistry software NOVA fitted the impedance spectrum (Version 2.1, Metrohm Autolab, Utrecht, Netherlands). A three-electrode cell was used, utilizing distinct surfaces as working electrodes. The reference and auxiliary electrodes employed were Ag/AgCl/KCl (saturated) and Pt wire, respectively.

The artificial saliva was prepared as mentioned in Table 1. That the pH was adjusted to 7.4.

## Result and discussion

### Surface characterization

The chemical structure of both samples, anodized titanium Ti-bare and coated Ti/CaPO<sub>4</sub>, were characterized by X-ray diffraction techniques. As represented in Fig. 1a, the XRD chart for anodized Ti surface. The characteristic peaks of titanium were observed at  $2\theta = 39.8, 52.3$  and  $71.1^\circ$  for attributed to miller indices (100), (200), and (211) respectively<sup>59,60</sup>. Accordingly, TiO<sub>2</sub> exists in crystal structure and point group of hexagonal and 6/mmm, respectively. Furthermore, the anatase titania (TiO<sub>2</sub>) phase formed via anodization was observed in Fig. 1a, which has three peaks at  $2\theta = 22.9, 38.2, 76.3$  for corresponding miller indices of (101), (004), and (211), respectively (JCPDS card no. 21-1272). The point group and crystal structure are recommended to be P<sub>4</sub>/mnm and tetragonal, respectively. As represented in Fig. 1b, the calcium triphosphate was characterized by the peaks at  $2\theta = 26.02, 31.6,$  and  $32.3^\circ$  for corresponding miller indices (002), (211), and (300)<sup>61,62</sup>. Whereas the space group and crystal structure are recommended to be R $\bar{3}m$  and Trigonal, respectively. Furthermore, the crystal structure of calcium phosphate consisted of two inequivalent Ca<sup>2+</sup> points. The Ca<sup>2+</sup> is bounded to six equivalent O<sup>2-</sup> atoms in the first site. Thus, the Ca-O bond lengths are equal to 2.46 Å. On the other hand, the second site of Ca<sup>2+</sup> atoms is bounded to 10 coordinate geometry to 10 oxide atoms (O<sup>2-</sup>). Hence, the Ca-O bond is ranging 2.25–2.72 Å. At the same time, the P-O is represented in short and long bond lengths equal to 1.54 and 1.56 Å, respectively<sup>63,64</sup>.

The bond stretching within the molecule of the prepared CaPO<sub>4</sub> was studied by the FT-IR spectroscopy method to determine the functional groups. As illustrated in Fig. 2a. The peaks in the range of 3427 cm<sup>-1</sup> and 1639.1 cm<sup>-1</sup> refer to O–H stretching vibration modes of adsorbed water traces<sup>65</sup>. In addition, the peaks at 1034 and 563.3 cm<sup>-1</sup> correspond to the orthophosphate group vibration modes<sup>66</sup>. Furthermore, the IR spectra for different essential oils were studied as represented in Fig. 2b. the peak observed at 3446 cm<sup>-1</sup> corresponding to the O–H stretching in water molecule on the surface<sup>44</sup>, else, the peak at wavenumber equal to 2994, and 2820, and 1749 cm<sup>-1</sup> attributed to the functional groups of (sp<sup>3</sup>)C–H, and –(O=C–H) and C=O respectively<sup>67–69</sup>.

Composition	Potassium chloride	Calcium chloride dihydrate	Sodium chloride	Potassium phosphate monobasic	Sodium phosphate dibasic	Potassium bicarbonate	Potassium thiocyanate	Citric acid
Conc. (g/L)	0.720	0.220	0.600	0.680	0.866	1.500	0.060	0.03

**Table 1.** The composition of artificial saliva solution.

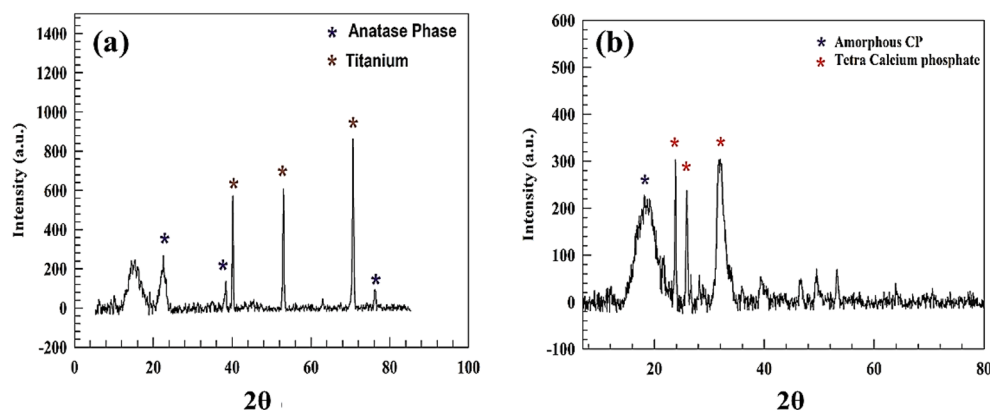


**Figure 1.** XRD chart of (a) Anodized Ti (Ti-bare), (b) Amorphous CaPO<sub>4</sub> nanoparticles ACP-NPs.

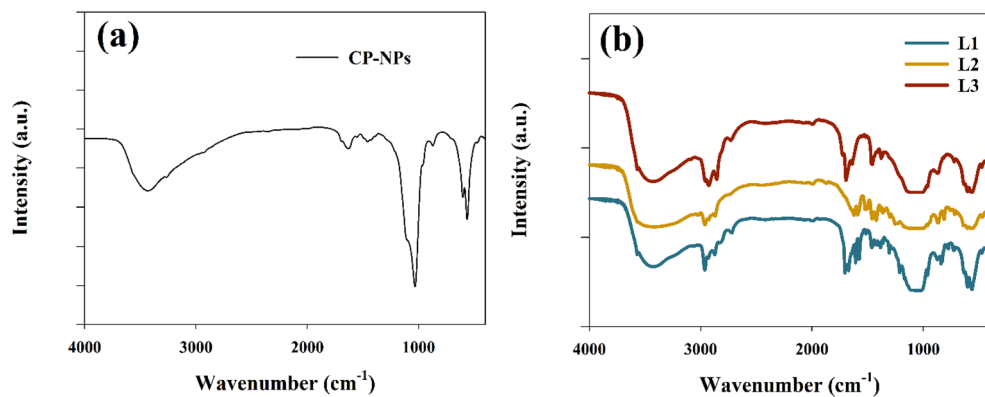


**Figure 2.** FT-IR- chart (a) Calcium Phosphate (CP-NPs), (b) Essential oils.

The surface morphology of the  $\text{CaPO}_4$ , which will deposit on the anodized Ti surface, was characterized by SEM, as represented in Fig. 3, at two different magnifications. As represented in Fig. 3, the nanosized  $\text{CaPO}_4$  particles were confirmed, and it was found to have a nano-flake shape and measured to be 60~80 nm. This figure illustrates more cavities on the surface, which increases the surface roughness, which is important to raise the biocompatibility of the Ti surface in saliva solution via increasing the corrosion resistance, as illustrated in the following sections. As we know, ACP is essential for the formation of mineralized bone and is used for bone substitutes<sup>70</sup>.

In the following sections, the electrochemical behavior of the anodized Ti/ $\text{CaPO}_4$  samples in compared with Ti-bare metal was investigated through the electrochemical impedance studies to estimate the corrosion resistance of these samples towards the simulated physiological solutions which containing the concentrations of salts and ions like; Cl, Na, P that play a responsible role in changing on the stability of these surfaces. We will discuss in detail the interpretation of the EIS measurements for the coated Ti/ $\text{CaPO}_4$  sample with or without the effect of essential oils (EO) in comparison with the Ti-bare sample. During the fitting process, the EIS data were fitted using ANOVA software, and the fitted circuit is illustrated in Fig. 4. The fitting model consists of solution resistance ( $R_s$ ) connected in series with ( $R_c/C$ ), where  $R_c$  is a charge transfer resistance, and C is a capacitor element. The presence of a constant phase element regards the naturally formed anatase layer ( $\text{TiO}_2$ ), as reported in the XRD part. Furthermore, the constant phase element of EIS is mathematically like the capacitor component. Where the following equation can employ the impedance of CPE<sup>71–73</sup>:

$$Z = (1/Y_0)/(j\omega)^n, \quad (1)$$

where the proportional factor ( $Y_0$ ) is the CPE constant, the angular frequency is ( $\omega$ ) (in radians/sec), the imaginary number  $j^2 = -1$ , and  $n$  is the CPE exponent ranges from zero to one.

Given the EIS Nyquist spectra of the present samples after 3 h of immersion in simulated saliva solution containing EO, was represented in Fig. 5. We noticed that the EO (L1 or L2 or L3) plays a great role in raising the corrosion resistance of the anodized Ti/ $\text{CaPO}_4$ . These results support our hypothesis that while the  $\text{CaPO}_4$  on anodized Ti acts as a bioactive coat, a synergistic effect emerges between the EO  $\text{CaPO}_4$ , acting as a superior for the stability of Ti sample in the oral environment. In the following sections, we will be giving more evidence

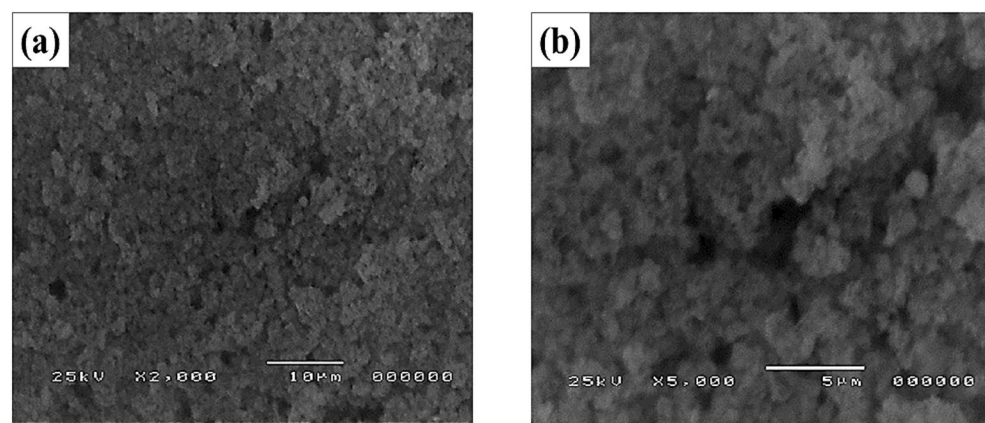


**Figure 3.** SEM Image of the amorphous  $\text{CaPO}_4$  on the anodized Ti surface.

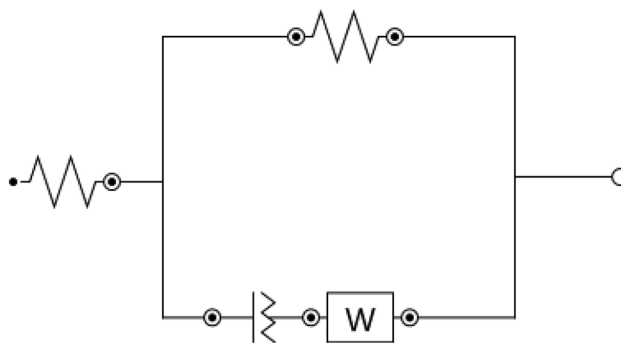


**Figure 4.** Fitting circuit of the EIS data.

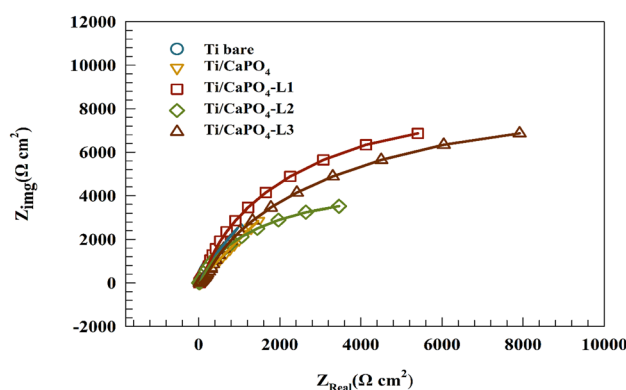


**Figure 5.** Comparison of different modified  $\text{CaPO}_4$  Ti surfaces in simulated saliva solution (i.e., Ti-bare, Ti/ $\text{CaPO}_4$ , Ti/ $\text{CaPO}_4$ -L1, Ti/ $\text{CaPO}_4$ -L2, Ti/ $\text{CaPO}_4$ -L3).

to confirm the synergistic relation between the  $\text{CaPO}_4$  on the surface and the EO in the solution to prove its positive impact on the corrosion resistance of Ti in simulated solutions. For this reason, we will discuss two categories of EIS measurements. The first one focuses on the study of the electrochemical behavior of Ti/ $\text{CaPO}_4$  in comparison to Ti-bare sample without the addition of EO in saliva solution for two periods, a short time of 240 min and a long time of 336 h. In the second category, we study the effect of the addition of EO in the solution for the same two periods.

Figure 6a,b shows the Nyquist plot of the Ti-bare and Ti/ $\text{CaPO}_4$  surface through 240 min. As represented in Fig. 6a, the Nyquist plot of Ti-bare in saliva solution shows the increase of resistance by time of soaking. As appeared in Fig. 6b, the value of the impedance increases in the resistive component, which indicates that the  $\text{CaPO}_4$  coat enhances the corrosion resistance by improving the surface compatibility<sup>74</sup>.

A comparison between the charge transfer resistance, calculated over different time intervals for Ti-bare and Ti/ $\text{CaPO}_4$  electrodes, was represented in (Fig. 6c). Where the  $R_{ct}$  values for Ti-bare are less than Ti/ $\text{CaPO}_4$  values, this explains the role of  $\text{CaPO}_4$  in enhancing the corrosion resistance between the coating and Ti surface in saliva solution. Additionally, the fitting parameters of Ti-bare and modified Ti/ $\text{CaPO}_4$  by using the fitting circuit appeared in Fig. 4, are represented in Tables 2 and 3. From this Table, we can deduce the many important features as the resistance of Ti-bare redouble from 424  $\Omega$  to 844  $\Omega$  after 240 min (Table 2), while for Ti/ $\text{CaPO}_4$  it 4 times multiplied during the same time, where the resistance increases from 460.08 to 1875.3  $\Omega$  (Table 3). Also, the high-value  $R_s$  values of Ti-bare than Ti/ $\text{CaPO}_4$  samples refers to the role of  $\text{CaPO}_4$  to decrease the  $R_s$  values during the time of immersion, which means that the good migration of the ions to the surface. The small capacitance value C points to the low capability of the surface to store charge. This result supports the good corrosion resistance of the surfaces where the capacitance is inversely proportional to the resistance<sup>70</sup>.

The effect of increasing the time of immersion from 240 min to 336 h or 14 days was studied in this section. As seen in Fig. 7a,b, the Nyquist plot of the Ti-bare and Ti/ $\text{CaPO}_4$  after 14 days of soaking in the saliva solution (without EO). The linear Nyquist plot indicates a non-charge transfer process, whereas the process is mainly diffusion<sup>70</sup>. Another time, the increase of the corrosion resistance of the Ti/ $\text{CaPO}_4$  sample reflects the positive impact of the  $\text{CaPO}_4$  layer, where the coating layer promotes surface durability. In Fig. 7c, a comparison between the charge transfer resistance over different time intervals for Ti-bare and Ti/ $\text{CaPO}_4$  electrodes was studied, and the results indicated that the charge transfer resistance reached a steady state after 14 days of soaking in the saliva solution. The resulting EIS fitting parameters based on the same fitting circuit (Fig. 4) were reported in the Tables 4 and 5. Where the resistance increases from 2831 to 3985  $\Omega$  for Ti-bare and from 4624 to 6890  $\Omega$  for Ti/ $\text{CaPO}_4$  during 336 h.

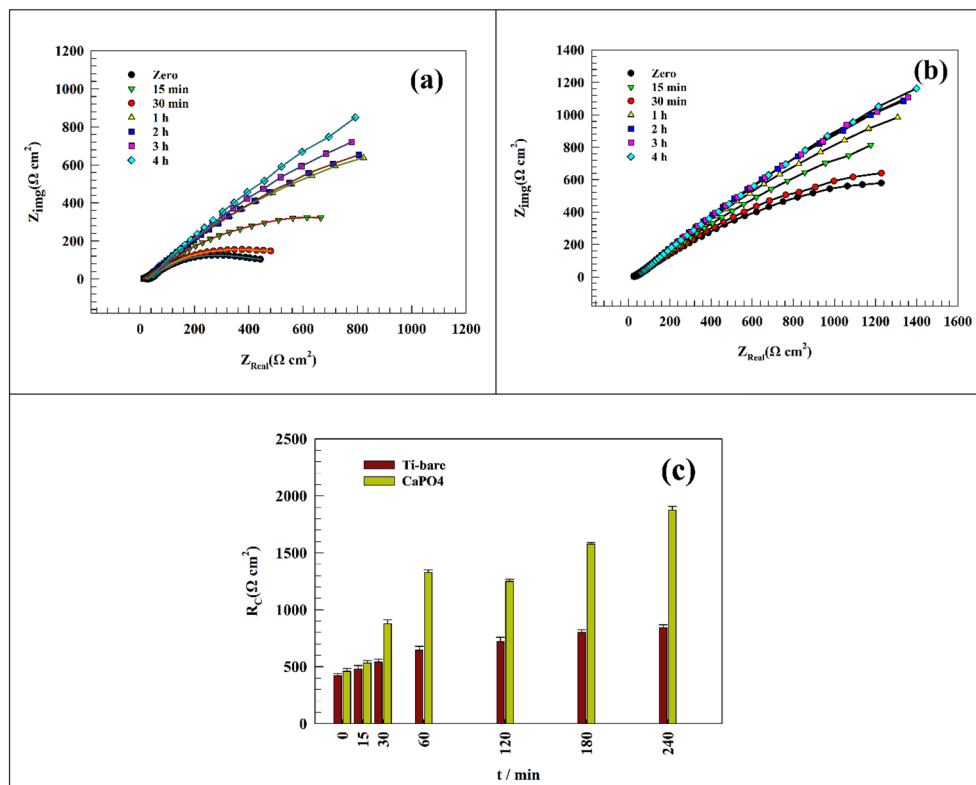


**Figure 6.** Representing of the Nyquist plot of the (a) Ti-bare and (b) Ti/CaPO<sub>4</sub> after soaking in saliva for 240 min. (c) Comparison between the charge transfer resistance at different time intervals.

Immersion time (min)	R <sub>s</sub> Ω cm <sup>2</sup>	R <sub>ct</sub> Ω cm <sup>2</sup>	C (F)	w Y <sub>0</sub>
Zero	25.3	424	0.0019465	0.0011911
15	22.98	479	0.0022877	0.0013932
30	21.85	541	0.0017624	0.001487
60	21.23	645	0.001549	0.0015886
120	13.65	721	0.0022474	0.0014037
180	31.21	801	0.0016422	0.0017883
240	29.51	844	0.0015989	0.0017496

**Table 2.** Representation of the fitting parameters of Ti-bare electrode for 240 min in simulated saliva solution.

Immersion time (min)	R <sub>s</sub> Ω cm <sup>2</sup>	R <sub>ct</sub> Ω cm <sup>2</sup>	C (F)	w Y <sub>0</sub>
Zero	20.31	460.08	0.0087754	0.00066173
15	18.75	534.9	0.0087735	0.00098218
30	18.34	878.4	0.0087121	0.00070918
60	23.96	1329.3	0.0081457	0.00106471
120	18.56	1250.1	0.0066522	0.00108867
180	18.21	1577.4	0.0083068	0.00104972
240	17.6	1675.3	0.0064027	0.00099656

**Table 3.** Representation of Ti/CaPO<sub>4</sub> electrode fitting parameters for 240 min in simulated saliva solution.

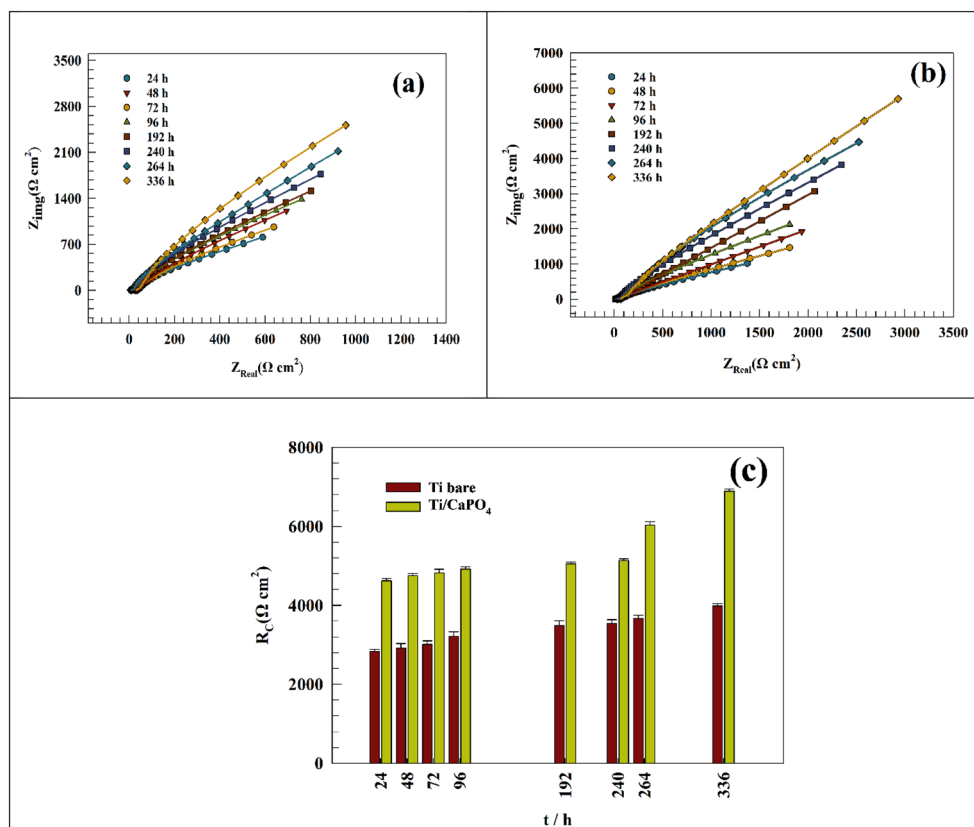


**Figure 7.** Representing of the Nyquist plot of the (a) Ti-bare and (b) Ti/CaPO<sub>4</sub> after soaking in saliva for 336 h. (c) Comparison between the charge transfer resistance at different time intervals.

Immersion time (hrs)	R <sub>s</sub>	R <sub>ct</sub>	C	w
	Ω cm <sup>2</sup>	Ω cm <sup>2</sup>	(F)	Y <sub>o</sub>
24	13.1	2831	0.0010499	0.0037738
48	27.2	2921	0.0010345	0.0036871
72	12.2	3013	0.0010318	0.0034524
96	7.3	3214	0.0010199	0.0032382
192	17.6	3487	0.0007478	0.0031025
240	11.9	3548	0.0005098	0.0020324
264	26.4	3672	0.0004855	0.0020198
336	28.8	3985	0.0003057	0.0020054

**Table 4.** Representation of the fitting parameters of Ti—bare electrode for 336 h in simulated saliva solution.

In this section, and for further enhancement of the corrosion resistance of the coated Ti/CaPO<sub>4</sub> surfaces. Three EO were used for medical applications, named Cumin, Thyme, and Coriander oils (L1, L2, and L3). They injected into the operating solution. The effect of EO was studied over two periods, 240 min and 336 h, to compare the result of the same electrodes in the presence of the green extract. As represented in Fig. 8, the comparison between the effect of concentration of three EO on the charge transfer resistance R<sub>ct</sub> of Ti/CaPO<sub>4</sub> appeared. Whereas different oil concentrations were used, i.e., 0.25% up to 2% (Wt/Wt). R<sub>ct</sub> of Ti/CaPO<sub>4</sub> was observed to increase by 264.4, 88.2, and 437.5% for L1, L2, and L3, respectively, at 2% of EO concentration.

As illustrated in Fig. 9a–c, the Nyquist plot of modified Ti/CaPO<sub>4</sub> electrode in saliva solution in the presence of 2.0% of different essential oils (L1, L2, and L3) for different time intervals up to 4 h. of soaking. However, the oil started diffusion with time, and the oil adsorption on the electrode surface enhanced the corrosion resistance over time. Hence, the diffusion of the saliva solution to the inner layers of the Ti sheet promotes the layer of the anodized Ti form, which is important for the corrosion resistance process. The progress of charge transfer resistance for each oil was followed as represented in Fig. 9d. By fitting the EIS result based on the fitting circuit (Fig. 4) for the Nyquist data, the R<sub>ct</sub> of the electrodes increased by 85, 27, and 33% for L1, L2, and L3, respectively.

Immersion time (hrs)	Rs	Rct	C	w
	$\Omega \text{ cm}^2$	$\Omega \text{ cm}^2$	(F)	$\Upsilon_o$
24	13.7	4624	0.0013603	0.0023142
48	6.9331	4752	0.0017779	0.0010329
72	13.713	4823	0.0009519	0.0014964
96	18.326	4919	0.0010911	0.0013919
192	14.229	5052	0.0010391	0.0014489
240	13.241	5137.5	0.0011269	0.0018313
264	18.21	6033.2	0.0007816	0.0014469
336	11.45	6890.2	0.0008409	0.0013728

**Table 5.** Representation of Ti /CaPO<sub>4</sub> electrode fitting parameters for 336 h in simulated saliva solution.

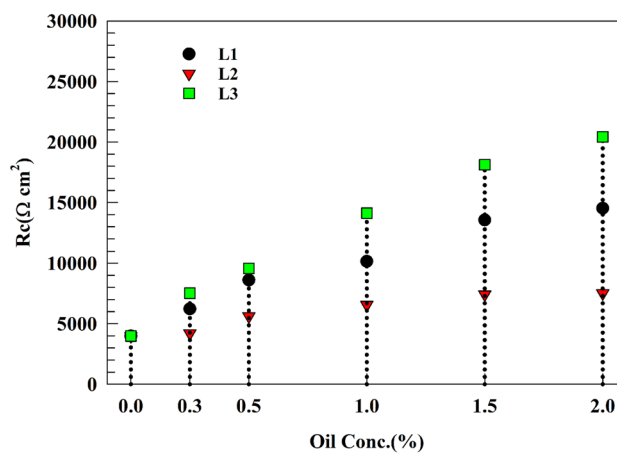


**Figure 8.** Comparison between the effect of essential oils concentration on Ti/CaPO<sub>4</sub> and charge transfer resistance after soaking 336 h in saliva solution.

The change in the charge transfer value reflects the different abilities of an oil to be adsorbed on the Ti surface. Whereas the oil ingredients are different in chemical structures. The fitting parameters extracted from Nyquist plots are represented in Tables 6, 7 and 8.

The modified electrode Ti/CaPO<sub>4</sub> was investigated in saliva solution and injected oils for 14 days (see Fig. 10a,c). After the 336 h of soaking of Ti/CaPO<sub>4</sub> in saliva, the electrode resistance started to reach the steady state where the charge transfer resistance was slightly changed. In the last 7 days, the resistance changed by 1.9, 7, and 2.8% for L1, L2, and L3, respectively. The anticorrosion activity of the EO was in the order of L3 > L1 > L2. The steric hindrance of the active component in the essential oils plays an important role in corrosion inhibition. For L3 oil, the most common ingredient, linalool, is long-chain alcohol, which has a smaller molecular volume than the bulky Thymol group (L2). The bulky group around the oxygen atom in thymol decreases the ability of thymol to be adsorbed on the titanium surface and diffusion through the CaPO<sub>4</sub> layer. As shown in Tables 9, 10 and 11, the EIS-relevant data were reported for different essential oils corresponding to the different time intervals. The progress of charge transfer resistance for each oil was shown in Fig. 10d, where the promising effect of L3 & L1 appeared and reached the high value after 72 h to be stable at 336 h. Although the value of the corrosion resistance is nearly the same for both L3 & L1 at the beginning of soaking (8166.5 & 8405  $\Omega$ , respectively), it doubles more than twice in the case of the L3 (20421  $\Omega$ ), compared to one and half times in the case of L1 (14,523  $\Omega$ ) after 336 h at the ending soaking. While the L2 oil increases the corrosion resistance with low value in comparison to L1 & L3, the progress of the resistance tripled through the time of soaking from 2680 to 7525  $\Omega$ .

### Polarization technique

The Tafel technique was used to prove the best behavior of surfaces in saliva solution after 14 days of immersion. As represented in Fig. 11, the linear polarization curve of different modified electrodes Ti-bare, Ti/CaPO<sub>4</sub>, Ti/CaPO<sub>4</sub>-L1, Ti/CaPO<sub>4</sub>-L2, and Ti/CaPO<sub>4</sub>-L3 at a scan of 1 mV s<sup>-1</sup> within potential window -1 to 1 V vs. the open circuit potential. The linear polarization data can estimate the Tafel slopes ( $\beta_a$  and  $\beta_c$ ). Furthermore, the values of corrosion current density ( $I_{corr}$ ) and corrosion potential ( $E_{corr}$ ) can be calculated by the interception of Tafel lines as listed in Table 12. The coated Ti/CaPO<sub>4</sub> showed more positive corrosion current ( $E_{corr}$ ) values than the Ti-bare electrode, indicating that lower corrosion rate, which is less favored upon these surfaces. On the other hand, the corrosion current is a value that reflects the actual corrosion rate. The electrode with a higher corrosion

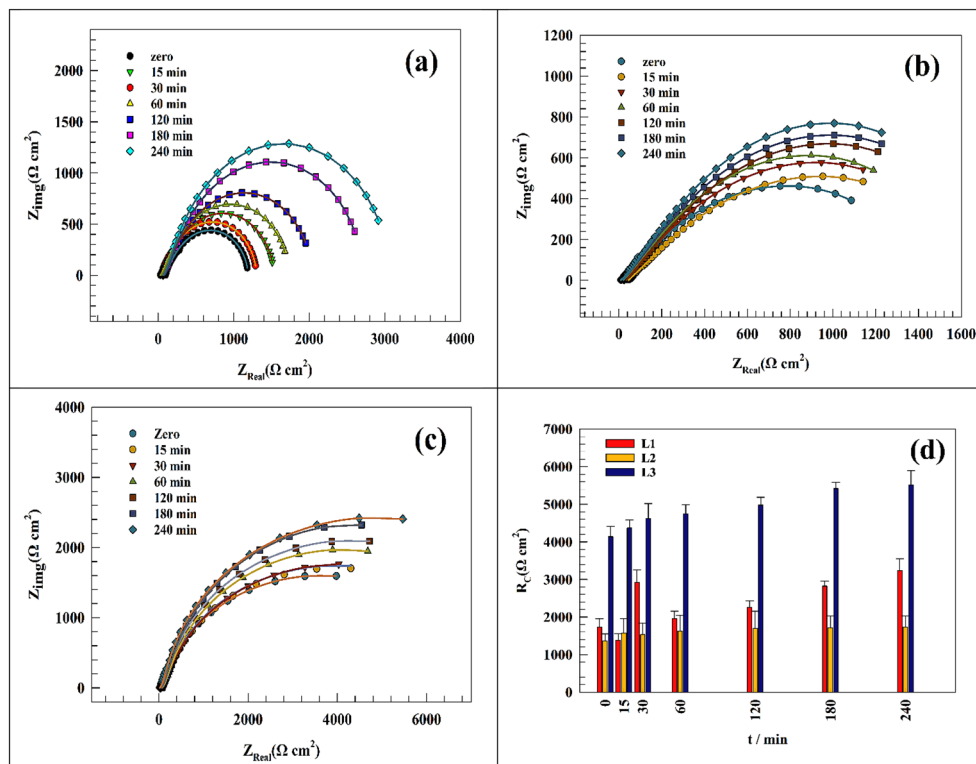


**Figure 9.** Representing of the Nyquist plot of the (a) Ti/CaPO<sub>4</sub>-L1, (b) Ti/CaPO<sub>4</sub>-L2, and (c) Ti/CaPO<sub>4</sub>-L3 after soaking in saliva for 240 min. (d) Comparison between the charge transfer resistance at different time intervals.

Immersion time (min)	Rs Ω cm <sup>2</sup>	Rct Ω cm <sup>2</sup>	C (F)	w Y <sub>o</sub>
Zero	20.31	1278	0.00010635	0.00094051
15	32.95	1378	0.00012117	0.00080105
30	80.82	2928	0.00010347	0.00080572
60	28.32	1955	0.00099075	0.00088006
120	51.84	2256	0.00010146	0.00082697
180	79.44	2826	0.0001137	0.00078212
240	65.39	3234	0.00010993	0.00082703

**Table 6.** Representation of the fitting parameters of Ti/CaPO<sub>4</sub> electrode for 240 min in simulated saliva solution in the presence of oil L1.

Immersion time (min)	Rs Ω cm <sup>2</sup>	Rct Ω cm <sup>2</sup>	C (F)	w Y <sub>o</sub>
Zero	8.1	1363.5	0.00072305	0.0009921
15	21.3	1571.8	0.00088464	0.00096715
30	26.5	1531	0.00097682	0.00090402
60	34.74	1634	0.00095467	0.00093186
120	21.1	1695	0.00070791	0.00100214
180	31.4	1713	0.00083436	0.00094872
240	27.1	1734	0.00079157	0.0009859

**Table 7.** Representation of the fitting parameters of Ti/CaPO<sub>4</sub> electrode for 240 min in simulated saliva solution in the presence of oil L2.

Immersion time (min)	Rs	Rct	C	w
	$\Omega \text{ cm}^2$	$\Omega \text{ cm}^2$	(F)	$Y_o$
Zero	17.45	4140	0.00048172	0.00074208
15	38.16	4370	0.00057622	0.00066165
30	34.51	4621	0.00057219	0.00073426
60	34.12	4751	0.00060768	0.00067721
120	42.14	4982	0.00063483	0.00073281
180	31.41	5421	0.00060124	0.00073165
240	34.72	5520	0.00059045	0.00073124

**Table 8.** Representation of the fitting parameters of Ti/CaPO<sub>4</sub> electrode for 240 min in simulated saliva solution in the presence of oil L3.

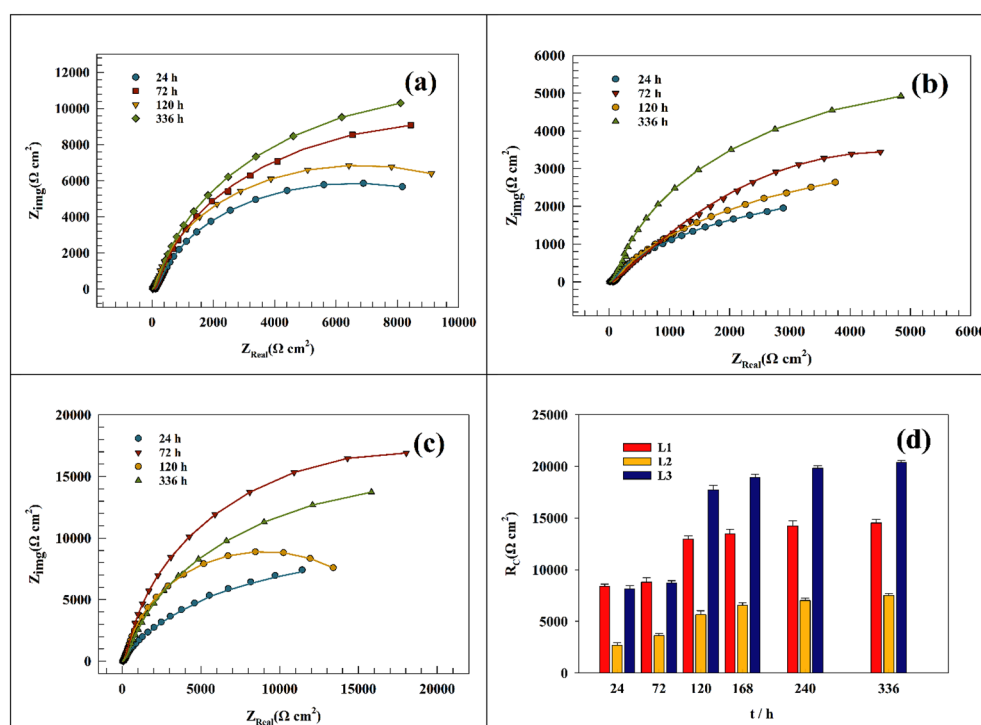


**Figure 10.** Representing of the Nyquist plot of the (a) Ti/CaPO<sub>4</sub>-L1, (b) Ti/CaPO<sub>4</sub>-L2, (c) Ti/CaPO<sub>4</sub>-L3 after soaking in saliva for 336 h (d) Comparison between the charge transfer resistance at different time intervals.

Immersion time (h)	Rs	Rct	C	w
	$\Omega \text{ cm}^2$	$\Omega \text{ cm}^2$	F	$Y_o$
24	20.31	8405	0.00014939	0.0012252
72	10.12	8810	0.00012538	0.001392
120	18.34	12,954	0.00015158	0.0013833
336	23.96	14,523	0.00013158	0.0010647

**Table 9.** Representation of the fitting parameters of Ti/CaPO<sub>4</sub> electrode for 336 h in simulated saliva solution in the presence of oil L1.

current indicates a higher corrosion rate. The effect of essential oil addition was observed for the following modified surfaces: Ti/CaPO<sub>4</sub>-L1, Ti/CaPO<sub>4</sub>-L2, and Ti/CaPO<sub>4</sub>-L3. Whereas the  $E_{\text{corr}}$  of the modified electrode showed an order of  $L3 > L2 > L1$ , this result is equivalent to the result deduced from the EIS results. Furthermore, the polarization resistance reflects the current flow rate caused by electrochemical reactions. The sample with higher polarization resistance matched the sample with higher corrosion resistance. Also, the corrosion rates of

Immersion time (h)	R <sub>s</sub>	R <sub>ct</sub>	C	w
	Ω cm <sup>2</sup>	Ω cm <sup>2</sup>	F	Y <sub>0</sub>
24	10.45	2680.83	0.00026199	0.00098412
72	51.54	3618.72	0.00022871	0.0008737
120	40.52	5647.54	0.00024685	0.00033963
336	35.55	7525.19	0.00013158	0.0010647

**Table 10.** Representation of the fitting parameters of Ti/CaPO<sub>4</sub> electrode for 336 h. in simulated saliva solution in the presence of oil L2.

Immersion time (h)	R <sub>s</sub>	R <sub>ct</sub>	C	w
	Ω cm <sup>2</sup>	Ω cm <sup>2</sup>	F	Y <sub>0</sub>
24	18.56	8166.5	0.00009636	0.0010891
72	19.92	8696.5	0.00010278	0.0010288
120	37.75	17,718	0.00009298	0.0010661
336	35.55	20,421	0.00009821	0.0010414

**Table 11.** Representation of the fitting parameters of Ti/CaPO<sub>4</sub> electrode for 336 h in simulated saliva solution in the presence of oil L3.

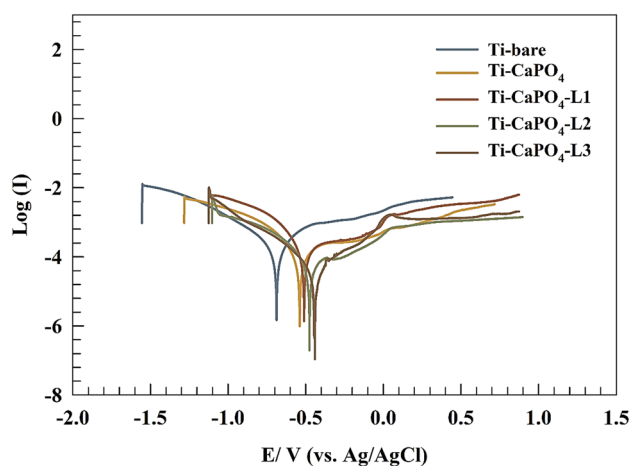


**Figure 11.** Polarization curves of different modified surfaces in saliva solution.

Electrode	$E_{Corr}(V)$	$I_{Corr}(A/cm^2) \times 10^{-5}$	Corrosion rate(mm/Year)	Polarization resistance
Ti-bare	-0.68737	8.74	1.015919	298.0441
Ti/CaPO <sub>4</sub>	-0.63884	7.25	0.640581	497.4933
Ti/CaPO <sub>4</sub> -L1	-0.56587	5.28	0.613117	453.8515
Ti/CaPO <sub>4</sub> -L2	-0.53073	4.62	0.520019	502.1876
Ti/CaPO <sub>4</sub> -L3	-0.47607	3.47	0.403613	750.1955

**Table 12.** Represents the polarization parameters for Ti-bare, Ti/CaPO<sub>4</sub>, Ti/CaPO<sub>4</sub>-L1, Ti/CaPO<sub>4</sub>-L2, Ti/CaPO<sub>4</sub>-L3.

each electrode were estimated using NOVA software based on the polarization data (See Table 12). The corrosion rate was expressed as mm of Ti foil per year (time interval). The electrode loss by corrosion in saliva fluid was Ti/bare > Ti/CaPO<sub>4</sub> > Ti/CaPO<sub>4</sub>-L1 > Ti/CaPO<sub>4</sub>-L2 > Ti-CaPO<sub>4</sub>-L3 due to the adsorption of EO on modified Ti/CaPO<sub>4</sub> surface.

## Conclusion

The findings of a recent study demonstrated that the development of a titanium surface for use in dental implant applications is not solely dependent on the type of surface modification used, but also on other aspects that may synergize with the modified materials to increase the implant's stability in the oral environment. The following is a reasonable inference to make considering the current results:

- 1- Anodization is still a simple electrochemical method used to treat the Ti surface to be active for further coating via the formation of a TiO<sub>2</sub> thick layer.
- 2- Anodized Ti-bare sample has high corrosion resistance, especially after 336 h of immersion in saliva solution where it increases from 844 to 3985 ohms.
- 3- ACP-NPs were used to prepare nano flaks structure from the CaPO<sub>4</sub> coat on the Ti implant.
- 4- The prepared Ti/CaPO<sub>4</sub> sample is considered a good bioactive surface. It increases the corrosion resistance from 460 to 1675 Ω after 240 min and to 6890 Ω after 336 h of immersion in saliva solution.
- 5- Selected three EOs added to saliva solution, Cumin, Thyme, and Coriander, synergized with the CaPO<sub>4</sub> coat on the Ti surface to enhance its stability by increasing the corrosion resistance to new high values equal to 14,523, 7525, and 20,421, respectively, after 336 h. of immersion in saliva solution.

Coriander, Thyme, and Cumin were found to have the most synergistic impact when stacked in that sequence. As a result, the chemical structure of the substance found in the oil might be utilised to explain the order in which the ability to preserve Ti/CaPO<sub>4</sub> is ranked. Coriander has a chemical that has a linear structure, and this structure improves the capacity of ions to diffuse through the CaPO<sub>4</sub> layer, which in turn raises the corrosion resistance. Despite the cumin compound's bulky structure's ability to restrict diffusion, the compound's resistance to corrosion actually reduced.

## Data availability

The datasets used and/or analyzed during the current study are available from the corresponding Author on reasonable request.

Received: 13 October 2023; Accepted: 12 January 2024

Published online: 18 January 2024

## References

1. Featherstone, J. D. B. Prevention and reversal of dental caries: Role of low level fluoride. *Community Dent. Oral Epidemiol.* **27**, 31–40 (1999).
2. Featherstone, J. D. B. The continuum of dental caries—Evidence for a dynamic disease process. *J. Dent. Res.* **83**, 39–42 (2004).
3. Selwitz, R. H., Ismail, A. I. & Pitts, N. B. Dental caries. *Lancet* **369**, 51–59 (2007).
4. Featherstone, J. D. B. Dental caries: A dynamic disease process. *Aust. Dent. J.* **53**, 286–291 (2008).
5. Chen, W. & Zhou, Y. Caries outcomes after orthodontic treatment with fixed appliances: A longitudinal prospective study. *Int. J. Clin. Exp. Med.* **8**, 2815 (2015).
6. Pakravanan, K., Rezaee Roknabadi, M., Farzanegan, F., Hashemzadeh, A. & Darroudi, M. Amorphous calcium phosphate nanoparticles-based mouthwash: Preparation, characterization, and anti-bacterial effects. *Green Chem. Lett. Rev.* **12**, 278–285 (2019).
7. Silva, R. C. S. *et al.* Titanium dental implants: An overview of applied nanobiotechnology to improve biocompatibility and prevent infections. *Materials (Basel)* **15**, 3150 (2022).
8. Du, Z. *et al.* Rolling reduction-dependent deformation mechanisms and tensile properties in a β titanium alloy. *J. Mater. Sci. Technol.* **104**, 183–193 (2022).
9. Cui, S. *et al.* Design and preparation of a biomedical titanium alloy with low elastic modulus and high antibacterial property based on Ti-Mo-Ag system. *J. Alloys Compd.* **908**, 164639 (2022).
10. Emiralioglu, A., Ünal, R. Additive manufacturing of gamma titanium aluminide alloys: A review. *J. Mater. Sci.* 1–26 (2022).
11. Nowruzzi, F., Imani, R. & Faghihi, S. Effect of electrochemical oxidation and drug loading on the antibacterial properties and cell biocompatibility of titanium substrates. *Sci. Rep.* **12**, 1–13 (2022).
12. Pantović Pavlović, M. R. *et al.* Anodizing/anaphoretic electrodeposition of nano-calcium phosphate/chitosan lactate multifunctional coatings on titanium with advanced corrosion resistance, bioactivity, and antibacterial properties. *ACS Biomater. Sci. Eng.* **7**, 3088–3102. <https://doi.org/10.1021/acsbomaterials.1c00035> (2021).
13. Lin, M.-H. *et al.* Improvement in bioactivity and corrosion resistance of Ti by hydroxyapatite deposition using ultrasonic mechanical coating and armoring. *Ceram. Int.* **48**, 4999–5008. <https://doi.org/10.1016/j.ceramint.2021.11.037> (2022).
14. Kazantseva, E.A., Komarova, E.G., Khimich, M.A. Structured and phase construction of zinc, strontium and silicon-containing micro-arc calcium phosphate coating, in: AIP Conf. Proc., AIP Publishing LLC, p. 20102 (2022).
15. Cheng, M.-S. *et al.* Preparation of calcium phosphate compounds on zirconia surfaces for dental implant applications. *Int. J. Mol. Sci.* **23**, 6675 (2022).
16. Zai, W., Sun, S., Man, H. C., Lian, J. & Zhang, Y. Preparation and anticorrosion properties of electrodeposited calcium phosphate (CaP) coatings on Mg–Zn–Ca metallic glass. *Mater. Chem. Phys.* **290**, 126532 (2022).
17. Barrere, F., Snel, M. M. E., van Blitterswijk, C. A., de Groot, K. & Layrolle, P. Nano-scale study of the nucleation and growth of calcium phosphate coating on titanium implants. *Biomaterials* **25**, 2901–2910. <https://doi.org/10.1016/j.biomaterials.2003.09.063> (2004).
18. Bashal, A. H. *et al.* Green synthesis of NiFe<sub>2</sub>O<sub>4</sub> nano-spinel oxide-decorated carbon nanotubes for efficient capacitive performance—Effect of electrolyte concentration. *Nanomaterials* **13**, 2643. <https://doi.org/10.3390/nano13192643> (2023).
19. Alamro, F. S. *et al.* Chitosan supports boosting NiCo<sub>2</sub>O<sub>4</sub> for catalyzed urea electrochemical removal application. *Polymers (Basel)* **15**, 3058. <https://doi.org/10.3390/polym15143058> (2023).
20. Hefnawy, M. A., Nafady, A., Mohamed, S. K. & Medany, S. S. Facile green synthesis of Ag/carbon nanotubes composite for efficient water splitting applications. *Synth. Met.* **294**, 117310. <https://doi.org/10.1016/j.synthmet.2023.117310> (2023).
21. Attia, N. M. & Ramadan, R. I. In vitro remineralizing effect of some herbals on initial enamel carious lesions. *Al-Azhar. Dent. J. Girls* **8**, 325–333 (2021).
22. Rani, B. E. A. & Basu, B. B. J. Green inhibitors for corrosion protection of metals and alloys: An overview. *Int. J. Corros.* **2012**, 380217. <https://doi.org/10.1155/2012/380217> (2012).

23. Ebenso, E. E. & Ekpe, U. J. Kinetic study of corrosion and corrosion inhibition of mild steel in H<sub>2</sub>SO<sub>4</sub> using Carica papaya leaves extract. *West African J. Biol. Appl. Chem.* **41**, 21–27 (1996).
24. Ebenso, E. E. *et al.* Corrosion inhibition studies of some plant extracts on aluminium in acidic medium. *Trans. Adv. Electrochem. Sci. Technol.* **39**, 117 (2004).
25. Kliškić, M., Radošević, J., Gudić, S. & Katalinić, V. Aqueous extract of Rosmarinus officinalis L. as inhibitor of Al–Mg alloy corrosion in chloride solution. *J. Appl. Electrochem.* **30**, 823–830 (2000).
26. Abiola, O. K., Oforka, N. C., Ebenso, E. E. & Nwinuka, N. M. Eco-friendly corrosion inhibitors: The inhibitive action of extract for the corrosion of aluminium in acidic media. *Anti-Corros. Methods Mater.* **54**, 219–224. <https://doi.org/10.1108/00035590710762357> (2007).
27. Ekpe, U. J., Ebenso, E. E. & Ibok, U. J. Inhibitory action of Azadirachta indica leaves extract on the corrosion of mild steel in H<sub>2</sub>SO<sub>4</sub>. *JW Afr. Sci. Assoc.* **37**, 13–30 (1994).
28. Buhl, H. The corrosion and oxidation of metals. Von Utick R. Evans. (2nd Supplementary Volume). Edward Arnold (Publishers) Ltd., London, 1976. £ 27.50. *Mater. Corros.* **29**, 80. <https://doi.org/10.1002/mac0.19780290130> (1978).
29. Fiala, A., Chibani, A., Darchen, A., Boulkamh, A. & Djebbar, K. Investigations of the inhibition of copper corrosion in nitric acid solutions by ketene dithioacetal derivatives. *Appl. Surf. Sci.* **253**, 9347–9356 (2007).
30. Sowbhagya, H. B. Chemistry, technology, and nutraceutical functions of cumin (*Cuminum cyminum* L.): An overview. *Crit. Rev. Food Sci. Nutr.* **53**, 1–10 (2013).
31. El-Ghorab, A. H., Nauman, M., Anjum, F. M., Hussain, S. & Nadeem, M. A comparative study on chemical composition and antioxidant activity of ginger (*Zingiber officinale*) and cumin (*Cuminum cyminum*). *J. Agric. Food Chem.* **58**, 8231–8237 (2010).
32. Mnif, S. & Aifa, S. Cumin (*Cuminum cyminum* L.) from traditional uses to potential biomedical applications. *Chem. Biodivers.* **12**, 733–742. <https://doi.org/10.1002/cbdv.201400305> (2015).
33. Nagiub, A. M. Electrochemical noise analysis for different green corrosion inhibitors for copper exposed to chloride media. *Port. Electrochim. Acta* **35**, 201–210 (2017).
34. Idouhli, R., Abouelfida, A., Benyaich, A. & Aityoub, A. Cuminum cyminum extract—a green corrosion inhibitor of S300 steel in 1 M HCl. *Chem. Process Eng. Res.* **44**, 16–25 (2016).
35. Ladha, D. G., Naik, U. J. & Shah, N. K. Investigation of Cumin (*Cuminum Cyminum*) extract as an eco-friendly green corrosion inhibitor for pure Aluminium in Acid medium. *J. Mater. Environ. Sci.* **4**, 701–708 (2013).
36. Naghdi Badi, H., Yazdani, D., Ali, S. M. & Nazari, F. Effects of spacing and harvesting time on herbage yield and quality/quantity of oil in thyme, *Thymus vulgaris* L.. *Ind. Crops Prod.* **19**, 231–236. <https://doi.org/10.1016/j.indcrop.2003.10.005> (2004).
37. Okafor, P. C. & Apebende, E. A. Corrosion inhibition characteristics of Thymus vulgaris, Xylopi aethiopica and Zingiber officinale extracts on mild steel in H<sub>2</sub>SO<sub>4</sub> solutions. *Pigment Resin Technol.* **43**, 357–364 (2014).
38. El Hajjaji, F. *et al.* Application of essential oil of thyme vulgaris as green corrosion inhibitor for mild steel in 1 M HCl. *J. Mater. Environ. Sci.* **7**, 567–578 (2016).
39. Ehsani, A. *et al.* Evaluation of Thymus vulgaris plant extract as an eco-friendly corrosion inhibitor for stainless steel 304 in acidic solution by means of electrochemical impedance spectroscopy, electrochemical noise analysis and density functional theory. *J. Colloid Interface Sci.* **490**, 444–451 (2017).
40. Kadiri, L. *et al.* Coriandrum Sativum L. seeds extract as a novel green corrosion inhibitor for mild steel in 1.0 M hydrochloric and 0.5 M sulfuric solutions. *Anal. Bioanal. Electrochem.* **10**, 249–268 (2018).
41. Prabhu, D. & Rao, P. Coriandrum sativum L.—A novel green inhibitor for the corrosion inhibition of aluminium in 1.0 M phosphoric acid solution. *J. Environ. Chem. Eng.* **1**, 676–683 (2013).
42. Al-Senani, G. M., Al-Saeedi, S. & Al-Mufarij, R. Coriandrum sativum leaves extract (CSL) as an eco-friendly green inhibitor for corrosion of carbon steel in acidic media. *J. Mater. Environ. Sci.* **7**, 2240–2251 (2016).
43. Prabhu, D. & Padmalatha, R. Corrosion inhibition of 6063 aluminum alloy by Coriandrum sativum L seed extract in phosphoric acid medium. *J. Mater. Env. Sci.* **4**, 732–743 (2013).
44. Al-Kadhi, N. S. *et al.* Zinc nanocomposite supported chitosan for nitrite sensing and hydrogen evolution applications. *Polymers (Basel)* **15**, 2357. <https://doi.org/10.3390/polym15102357> (2023).
45. Hefnawy, M. A., Medany, S. S., Fadlallah, S. A., El-Sherif, R. M. & Hassan, S. S. Novel self-assembly Pd(II)-Schiff base complex modified glassy carbon electrode for electrochemical detection of paracetamol. *Electrocatalysis* <https://doi.org/10.1007/s12678-022-00741-7> (2022).
46. Eliwa, A. S. *et al.* Ultrasonic-assisted synthesis of nickel metal–organic framework for efficient urea removal and water splitting applications. *Synth. Met.* **294**, 117309. <https://doi.org/10.1016/j.synthmet.2023.117309> (2023).
47. Hefnawy, M. A., Fadlallah, S. A., El-Sherif, R. M. & Medany, S. S. Competition between enzymatic and non-enzymatic electrochemical determination of cholesterol. *J. Electroanal. Chem.* **930**, 117169. <https://doi.org/10.1016/j.jelechem.2023.117169> (2023).
48. Eliwa, A. S. *et al.* Synthesis and characterization of lead-based metal–organic framework nano-needles for effective water splitting application. *Sci. Rep.* **13**, 12531. <https://doi.org/10.1038/s41598-023-39697-z> (2023).
49. Al-Kadhi, N. S. *et al.* Polyaniline-supported nickel oxide flower for efficient nitrite electrochemical detection in water. *Polymers (Basel)* **15**, 1804. <https://doi.org/10.3390/polym15071804> (2023).
50. Gamal, H., Elshahawy, A. M., Medany, S. S., Hefnawy, M. A. & Shalaby, M. S. Recent advances of vanadium oxides and their derivatives in supercapacitor applications: A comprehensive review. *J. Energy Storage* **76**, 109788. <https://doi.org/10.1016/j.est.2023.109788> (2024).
51. Encinas-Sánchez, V., de Miguel, M. T., Lasanta, M. I., García-Martín, G. & Pérez, F. J. Electrochemical impedance spectroscopy (EIS): An efficient technique for monitoring corrosion processes in molten salt environments in CSP applications. *Sol. Energy Mater. Sol. Cells* **191**, 157–163. <https://doi.org/10.1016/j.solmat.2018.11.007> (2019).
52. Han, Y. *et al.* Electrochemical impedance spectroscopy (EIS): An efficiency method to monitor resin curing processes. *Sensors Actuators A Phys.* **250**, 78–86. <https://doi.org/10.1016/j.sna.2016.08.028> (2016).
53. Ribeiro, D. V., Souza, C. A. C. & Abrantes, J. C. C. Use of Electrochemical Impedance Spectroscopy (EIS) to monitoring the corrosion of reinforced concrete. *Rev. IBRACON Estruturas e Mater.* **8**, 529–546 (2015).
54. Ribeiro, D. V. & Abrantes, J. C. C. Application of electrochemical impedance spectroscopy (EIS) to monitor the corrosion of reinforced concrete: A new approach. *Constr. Build. Mater.* **111**, 98–104 (2016).
55. Nechache, A., Cassir, M. & Ringuedé, A. Solid oxide electrolysis cell analysis by means of electrochemical impedance spectroscopy: A review. *J. Power Sources* **258**, 164–181 (2014).
56. Medany, S. S. & Hefnawy, M. A. Nickel–cobalt oxide decorated Chitosan electrocatalyst for ethylene glycol oxidation. *Surf. Interfaces* **40**, 103077. <https://doi.org/10.1016/j.surfint.2023.103077> (2023).
57. Hefnawy, M. A., Medany, S. S., El-Sherif, R. M., El-Bagoury, N. & Fadlallah, S. A. High-performance IN738 superalloy derived from turbine blade waste for efficient ethanol, ethylene glycol, and urea electrooxidation. *J. Appl. Electrochem.* <https://doi.org/10.1007/s10800-023-01862-7> (2023).
58. Ezzat, N., Hefnawy, M. A., Medany, S. S., El-Sherif, R. M. & Fadlallah, S. A. Green synthesis of Ag nanoparticle supported on graphene oxide for efficient nitrite sensing in a water sample. *Sci. Rep.* **13**, 19441. <https://doi.org/10.1038/s41598-023-46409-0> (2023).

59. He, Y., Huang, W., Chen, R., Zhang, W. & Lin, H. Improved electrochemical performance of boron-doped diamond electrode depending on the structure of titanium substrate. *J. Electroanal. Chem.* **758**, 170–177. <https://doi.org/10.1016/j.jelechem.2015.08.017> (2015).
60. Abdelkader, N., Pflitsch, C., Brors, G., Curdts, B. & Atakan, B. Study of cavitation erosion experiments on thermally oxidized rutile phase TiO<sub>2</sub> films on stainless steel. *J. Eng. Mater. Technol.* **5**, 1–6. <https://doi.org/10.12691/materials-5-1-1> (2017).
61. Hung, I.-M., Shih, W.-J., Hon, M.-H. & Wang, M.-C. The properties of sintered calcium phosphate with [Ca]/[P]= 1.50. *Int. J. Mol. Sci.* **13**, 13569–13586 (2012).
62. Wang, X., Schröder, H. C. & Müller, W. E. G. Amorphous polyphosphate, a smart bioinspired nano-/bio-material for bone and cartilage regeneration: Towards a new paradigm in tissue engineering. *J. Mater. Chem. B* **6**, 2385–2412 (2018).
63. Moore, P. Complex crystal structures related to glaserite, K<sub>3</sub>Na (SO<sub>4</sub>)<sub>2</sub>: Evidence for very dense packings among oxysalts. *Bull. Miner.* **104**, 536–547 (1981).
64. Huang, Y. A study of some chemical inferences in atomic absorption spectroscopy: a thesis... for the degree of Master of Science in Chemistry, (1970).
65. Hefnawy, M. A., Medany, S. S., El-Sherif, R. M. & Fadlallah, S. A. NiO-MnOx/Polyaniline/graphite electrodes for urea electrocatalysis: Synergetic effect between polymorphs of MnOx and NiO. *ChemistrySelect* **7**, e202103735. <https://doi.org/10.1002/slct.202103735> (2022).
66. Guerra-López, J. *et al.* Effects of nickel on calcium phosphate formation. *J. Solid State Chem.* **151**, 163–169. <https://doi.org/10.1006/jssc.1999.8615> (2000).
67. El-Nahass, M. M., Kamel, M. A., El-Barbary, A. A., El-Mansy, M. A. M. & Ibrahim, M. FT-IR spectroscopic analyses of 3-Methyl-5-Pyrazolone (MP). *Spectrochim. Acta A Mol. Biomol. Spectrosc.* **111**, 37–41 (2013).
68. Singh, M., Zhou, N., Paul, D. K. & Klabunde, K. J. IR spectral evidence of aldol condensation: Acetaldehyde adsorption over TiO<sub>2</sub> surface. *J. Catal.* **260**, 371–379 (2008).
69. Pinchas, S. Infrared absorption of aldehydic CH group. *Anal. Chem.* **29**, 334–339 (1957).
70. Amin, M. A., Fadlallah, S. A. & Alosaimi, G. S. In situ aqueous synthesis of silver nanoparticles supported on titanium as active electrocatalyst for the hydrogen evolution reaction. *Int. J. Hydrogen Energy* **39**, 19519–19540 (2014).
71. Hefnawy, M. A., Medany, S. S., El-Sherif, R. M. & Fadlallah, S. A. Green synthesis of NiO/Fe<sub>3</sub>O<sub>4</sub>@chitosan composite catalyst based on graphite for urea electro-oxidation. *Mater. Chem. Phys.* **290**, 126603. <https://doi.org/10.1016/j.matchemphys.2022.126603> (2022).
72. Hefnawy, M. A., Fadlallah, S. A., El-Sherif, R. M. & Medany, S. S. Nickel-manganese double hydroxide mixed with reduced graphene oxide electrocatalyst for efficient ethylene glycol electrooxidation and hydrogen evolution reaction. *Synth. Met.* **282**, 116959. <https://doi.org/10.1016/j.synthmet.2021.116959> (2021).
73. Hefnawy, M. A., Fadlallah, S. A., El-Sherif, R. M. & Medany, S. S. Synergistic effect of Cu-doped NiO for enhancing urea electrooxidation: comparative electrochemical and DFT studies. *J. Alloys Compd.* **896**, 162857. <https://doi.org/10.1016/j.jallcom.2021.162857> (2021).
74. Almeraya Calderon, F. *et al.* Corrosion behavior of titanium and titanium alloys in ringer's solution. *Int. J. Electrochem. Sci.* **17**, 55. <https://doi.org/10.20964/2022.07.55> (2022).

## Acknowledgements

Many thanks to Cairo University for supporting the present work.

## Author contributions

All authors contributed in the writing & revision of the paper.

## Funding

Open access funding provided by The Science, Technology & Innovation Funding Authority (STDF) in cooperation with The Egyptian Knowledge Bank (EKB).

## Competing interests

The authors declare no competing interests.

## Additional information

**Correspondence** and requests for materials should be addressed to S.A.F.

**Reprints and permissions information** is available at [www.nature.com/reprints](http://www.nature.com/reprints).

**Publisher's note** Springer Nature remains neutral with regard to jurisdictional claims in published maps and institutional affiliations.



**Open Access** This article is licensed under a Creative Commons Attribution 4.0 International License, which permits use, sharing, adaptation, distribution and reproduction in any medium or format, as long as you give appropriate credit to the original author(s) and the source, provide a link to the Creative Commons licence, and indicate if changes were made. The images or other third party material in this article are included in the article's Creative Commons licence, unless indicated otherwise in a credit line to the material. If material is not included in the article's Creative Commons licence and your intended use is not permitted by statutory regulation or exceeds the permitted use, you will need to obtain permission directly from the copyright holder. To view a copy of this licence, visit <http://creativecommons.org/licenses/by/4.0/>.

© The Author(s) 2024

## Terms and Conditions

Springer Nature journal content, brought to you courtesy of Springer Nature Customer Service Center GmbH (“Springer Nature”).

Springer Nature supports a reasonable amount of sharing of research papers by authors, subscribers and authorised users (“Users”), for small-scale personal, non-commercial use provided that all copyright, trade and service marks and other proprietary notices are maintained. By accessing, sharing, receiving or otherwise using the Springer Nature journal content you agree to these terms of use (“Terms”). For these purposes, Springer Nature considers academic use (by researchers and students) to be non-commercial.

These Terms are supplementary and will apply in addition to any applicable website terms and conditions, a relevant site licence or a personal subscription. These Terms will prevail over any conflict or ambiguity with regards to the relevant terms, a site licence or a personal subscription (to the extent of the conflict or ambiguity only). For Creative Commons-licensed articles, the terms of the Creative Commons license used will apply.

We collect and use personal data to provide access to the Springer Nature journal content. We may also use these personal data internally within ResearchGate and Springer Nature and as agreed share it, in an anonymised way, for purposes of tracking, analysis and reporting. We will not otherwise disclose your personal data outside the ResearchGate or the Springer Nature group of companies unless we have your permission as detailed in the Privacy Policy.

While Users may use the Springer Nature journal content for small scale, personal non-commercial use, it is important to note that Users may not:

1. use such content for the purpose of providing other users with access on a regular or large scale basis or as a means to circumvent access control;
2. use such content where to do so would be considered a criminal or statutory offence in any jurisdiction, or gives rise to civil liability, or is otherwise unlawful;
3. falsely or misleadingly imply or suggest endorsement, approval, sponsorship, or association unless explicitly agreed to by Springer Nature in writing;
4. use bots or other automated methods to access the content or redirect messages
5. override any security feature or exclusionary protocol; or
6. share the content in order to create substitute for Springer Nature products or services or a systematic database of Springer Nature journal content.

In line with the restriction against commercial use, Springer Nature does not permit the creation of a product or service that creates revenue, royalties, rent or income from our content or its inclusion as part of a paid for service or for other commercial gain. Springer Nature journal content cannot be used for inter-library loans and librarians may not upload Springer Nature journal content on a large scale into their, or any other, institutional repository.

These terms of use are reviewed regularly and may be amended at any time. Springer Nature is not obligated to publish any information or content on this website and may remove it or features or functionality at our sole discretion, at any time with or without notice. Springer Nature may revoke this licence to you at any time and remove access to any copies of the Springer Nature journal content which have been saved.

To the fullest extent permitted by law, Springer Nature makes no warranties, representations or guarantees to Users, either express or implied with respect to the Springer nature journal content and all parties disclaim and waive any implied warranties or warranties imposed by law, including merchantability or fitness for any particular purpose.

Please note that these rights do not automatically extend to content, data or other material published by Springer Nature that may be licensed from third parties.

If you would like to use or distribute our Springer Nature journal content to a wider audience or on a regular basis or in any other manner not expressly permitted by these Terms, please contact Springer Nature at

[onlineservice@springernature.com](mailto:onlineservice@springernature.com)